Optimizing the deposition rate of vacuum-grown n-octylphosphonic acid monolayer for low-voltage thin-film transistors

S. Gupta, H. Gleskova

Department of Electronic and Electrical Engineering, University of Strathclyde, 204 George Street, Glasgow, G1 1XW, United Kingdom

Abstract

A self-assembled monolayer of n-octylphosphonic acid (C_8PA) is prepared from vapour phase in vacuum. C_8PA thickness corresponding to several monolayers is deposited on aluminium oxide (AlO_x) and subsequently heated to leave a monolayer of chemisorbed molecules.

The effect of C_8PA deposition rate on a 15-nm-thick, bi-layer AlO_x/C_8PA dielectric and low-voltage p-channel organic thin-film transistors (OTFTs) is studied. The increase in the deposition rate from 0.1 to 7.0 Å/s leads to increase in the field-effect mobility from 0.039 to 0.061 cm^2/Vs, while the threshold voltage remains around -1.55 V. At the same time, the off-current is reduced from 2.3×10^{-12} to 1.3×10^{-12}A, the subthreshold slope is lowered from 100 to 89 mV/decade and the on/off current ratio is increased from ~ 10^5 to ~ 10^6.

The leakage current density of AlO_x is reduced from 1×10^{-7} to 4×10^{-8} A/cm^2 at 3 V when C_8PA monolayer is added on top of it. In addition, pentacene grain size on AlO_x/C_8PA is larger than that on AlO_x. The overall performance of AlO_x/C_8PA OTFTs is superior to that of AlO_x OTFTs.

1. Introduction

Low processing temperature of organic thin-film transistors is compatible with plastic substrates for flexible active matrix displays [1]. Their high on/off current ratio and modest field-effect mobility are sufficient for non-emissive displays such as electrophoretic and liquid crystal [2]. Emissive displays, such as organic light-emitting diodes, require transistors with higher on-current and good bias stability. Since the drain current of a field-effect transistor is proportional to the capacitance of its gate dielectric, higher on-currents can be achieved by using dielectrics with high capacitance. Ultra-thin dielectrics based on materials with high- to moderate-k values, for example aluminium oxide [3, 4], lead to high capacitance; however, their leakage current must be controlled. The leakage current in excess of 10^{-6} A/cm^2 [5] of ultra-thin oxides can be reduced by functionalizing them with self-assembled monolayers (SAM) [6–11]. Along with the suppression of the leakage current, SAMs provide higher field-effect mobility than oxide surfaces [7, 11, 12]. Organic thin-film transistors (OTFTs) with SAMs achieved operating voltages less than 3 V [6–11].

The fabrication of display backplanes requires processes that produce layers with very high uniformity over large areas. Here, layer depositions with large process windows and self-limiting growth mechanisms provide an advantage. We developed a vacuum process for fabrication of an ultra-thin, bi-layer dielectric consisting of aluminium oxide (AlO_x) and n-octyl-phosphonic acid (C_8PA). AlO_x is prepared by UV/ozone oxidation of thermally evaporated aluminium [13]. C_8PA monolayer is prepared in two steps: firstly several monolayers are vapour-deposited on AlO_x in vacuum and then the substrate is heated to remove all physisorbed molecules [14]. However, the kinetics of the chemisorption process of the phosphonate group to AlO_x and the molecular alignment of C_8PA molecules are affected by the deposition temperature [15] and the post-annealing treatment [14]. This paper studies how the deposition rate of C_8PA affects the performance of organic thin-film transistors (OTFTs) and the corresponding metal-insulator-metal (MIM) structures.

2. Experimental details

MIM structures and OTFTs were fabricated side by side on Eagle 2000 glass substrate. Approximately a 15-nm-thick AlO_x was obtained by UV/ozone oxidation of thermally evaporated aluminium [13]. C_8PA corresponding to several monolayers was thermally evaporated at rates of 0.1, 1, 3, and 7 Å/s, respectively. Each C_8PA layer was desorbed at ~ 160°C for an hour. In OTFT structures, 50-nm-thick, four-time purified pentacene was deposited at room temperature. Finally, 50-nm-thick gold contacts were evaporated to complete the MIM and OTFT structures. The fabrication used vacuum-grown processes only, applying shadow masks where needed. The maximum process temperature was 160°C. The fabricated transistors have channel lengths of 30, 50, 70, and 90 μm and the channel width of 1000 μm. The transistor cross-section is shown in Figure 1. The reference MIM structures and OTFTs without C_8PA monolayer were also prepared. The dielectric with and without C_8PA monolayer is referred to as AlO_x/C_8PA and AlO_x, respectively.

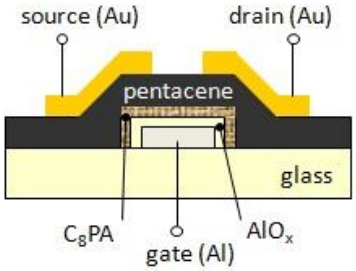

Figure 1: OTFT cross-section.

The capacitance of AlO_x and AlO_x/C_8PA dielectrics was measured from 1 kHz to 1 MHz and the current-voltage characteristic between 3 and -3 V.

OTFT transfer characteristics were measured at drain-to-source voltage (V_{DS}) of -0.1 and -3 V while sweeping the gate-to-source voltage (V_{GS}) from 1 to -3 V. The OTFT field-effect mobility (μ) and threshold voltage (V_{th}) were calculated from the transfer characteristics using the standard MOSFET equations. We define the off-current (I_{off}) and the on-current as the minimum and maximum drain current at V_{DS} = -3 V, respectively. The subthreshold slope ($S = \partial V_{GS}/\partial(\log I_D)$) is extracted from the slope of log I_D versus V_{GS}. The output characteristics were measured for V_{GS} of 0, -0.5, -1.0, -1.5, -2.0, -2.5, and -3.0, while sweeping V_{DS} between 0 and -3 V. Finally, the surface topography of pentacene was studied by atomic force microscopy (AFM) using the tapping mode.

3. Results and discussion

This section presents the properties of MIM and OTFT devices with AlO_x/C_8PA dielectric. Their properties were studied with respect to C_8PA deposition rate and the reference AlO_x devices.

3.1 Dielectric Properties

The mean and standard deviation of capacitances were calculated from several MIM structures and the values at 100 kHz are shown in Figure 2(a). Figure 2(b) presents the gate leakage current density of AlO_x/C_8PA and AlO_x dielectrics.

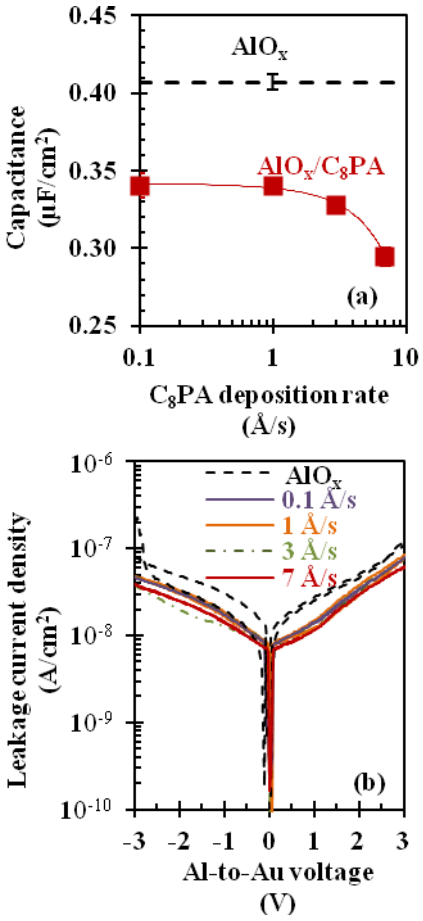

Figure 2: Capacitance (a) and leakage current density (b) of AlO_x/C_8PA bi-layer dielectric.

The capacitance of the AlO_x/C_8PA bi-layer dielectric is ~ 0.34 μF/cm^2 for C_8PA deposition rate of 0.1 Å/s. The capacitance slightly decreases with increasing C_8PA deposition rate, reaching a value of ~ 0.30 μF/cm^2 at the rate of 7 Å/s. The reference capacitance of AlO_x is ~ 0.41 μF/cm^2. The lower dielectric capacitance of AlO_x/C_8PA versus AlO_x confirms the presence of C_8PA for all deposition rates. Previously, we confirmed that C_8PA deposited in vacuum at a rate of 3 Å/s is chemically bonded to AlO_x [15]. Since the post-deposition annealing of the C_8PA layer at the temperature of ~ 160°C previously led to removal of all physisorbed C_8PA molecules, one would conclude that C_8PA molecules are chemically bonded to AlO_x regardless of their deposition rate. Nevertheless, the slightly lower capacitance obtained for higher deposition rate suggests a slightly larger thickness and/or lower relative permittivity of the organic monolayer.

The gate leakage current density of AlO_x/C_8PA and AlO_x are ~ 4×10^{-8} and ~1×10^{-7} A/cm^2 at 3 V, respectively. There is no observable difference in the gate leakage current density with deposition rate. The leakage current obtained with our vapour-deposited C_8PA monolayer is comparable to the solution processed alkyl phosphonic acid monolayers by Jedaa et al [6], Wöbkenberg et al. [10], Ma et al [11], and Klauk et al. [16].

3.2 OTFT characteristics

Figure 3 shows the transfer and output characteristics of OTFTs with C_8PA deposited at the rate of 7 Å/s. The channel width (W) and length (L) is 1000 and 30 μm, respectively. The drain current of AlO_x/C_8PA OTFTs is about four orders of magnitude higher than the gate current at V_{GS} = V_{DS} = -3.0 V. Also, the transistors have good linear and saturation characteristics.

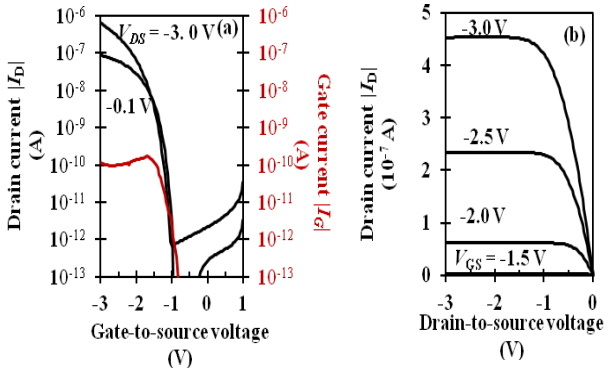

Figure 3: Transfer (a) and output (b) characteristics of AlO_x/C_8PA OTFTs.

3.3 OTFT parameters and pentacene morphology

The mean and standard deviation of field-effect mobility, threshold voltage, subthreshold slope, and off-current are presented in Figure 4 (a)-(d), respectively. On/off current ratio of transistors with 30 μm channel length is shown in Figure 5. Figure 6(a) shows the AFM surface image of 50-nm-thick pentacene deposited on AlO_x. Figure 6(b) shows the surface of the same pentacene layer grown on AlO_x/C_8PA with C_8PA deposited at the rate of 7 Å/s.

As shown in Figure 4(a), the field-effect mobility of AlO_x/C_8PA OTFTs increases from 0.039 to 0.061 cm^2/Vs as the C_8PA deposition rate increases from 0.1 to 7 Å/s. The mean field-effect mobility of the reference AlO_x OTFTs is ~ 0.038 cm^2/Vs. The threshold voltage is ~-1.55 V for all AlO_x/C_8PA OTFTs regardless of the C_8PA deposition rate. The mean threshold voltage of the reference AlO_x OTFTs is -1.75 V. The lower threshold voltage of AlO_x/C_8PA OTFTs is an advantage for low-voltage device operation [17].

The off-current of OTFTs with AlO_x is 3.2×10^{-12} A. The off-current is lower for AlO_x/C_8PA OTFTs; it decreases from 2.3×10^{-12} to 1.3×10^{-12} A with increasing C_8PA deposition rate. Similarly, the subthreshold slope of AlO_x/C_8PA OTFTs is reduced from 104 to 89 mV/decade with increasing C_8PA deposition rate, while the reference AlO_x OTFTs have the subthreshold slope of 105 mV/decade. At the deposition rate of 7 Å/s, the subthreshold slope is close to the best reported value for pentacene-based organic thin-film transistors [11, 16] and slightly higher than that reported by Acton et al. [18].

Figure 5 shows that the on/off current ratio is higher than 10^5 for all OTFTs with L = 30 μm and W = 1000 μm. At the lowest deposition rate, the current ratio of AlO_x/C_8PA OTFTs is 1.3×10^5, which is similar to that of AlO_x OTFTs; but it reaches almost 10^6 at the highest deposition rate. The higher field-effect mobility achieved at higher C_8PA deposition rate resulted in larger on-current and, consequently, higher on/off current ratio is achieved. The current ratio of 10^6 at the C_8PA deposition rate

of 7 Å/s is comparable to the best values reported previously for low-voltage OTFTs. In addition, it is similar to on/off current ratio obtained for alkyl phosphonic acids with intermediate alkyl chain length (10-14 carbon atoms) [6, 7, 19].

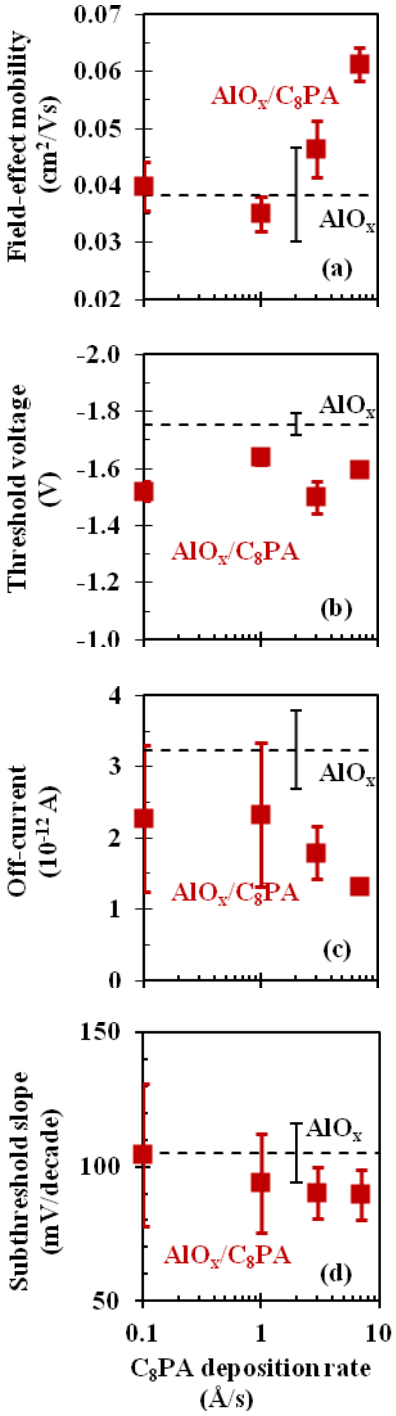

Figure 4: OTFT field-effect mobility (a), threshold voltage (b), off-current (c), and subthreshold slope (d) as functions of C_8PA evaporation rate. The reference aluminium oxide is presented as dashed line.

Pentacene grain size is less than 100 nm (see Figure 6(a)) when it is deposited on AlO_x. This small grain size is correlated with lower field-effect mobility of AlO_x OTFTs. Pentacene deposited on AlO_x/C_8PA surface exhibits different morphology with grain size of about150-200 nm (see Figure 6(b)). C_8PA deposition rate has only minor effect on pentacene morphology, even though the field-effect mobility in the corresponding OTFTs varies. This variation in the field-effect mobility could result from different C_8PA structural properties. Previously we observed that the C_8PA growth temperature affected the structural properties of the organic monolayer [15]. The effect of the C_8PA deposition rate on the structural properties of the self-assembled monolayer is under investigation.

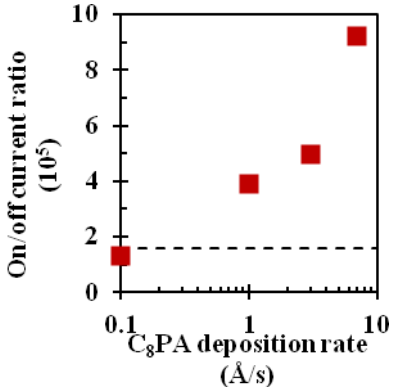

Figure 5: On/off current ratio of OTFTs with AlO_x/C_8PA and AlO_x (dashed line) gate dielectric. The channel width and length are 1000 and 30 µm, respectively.

Finally, the higher-field effect mobility achieved with AlO_x/C_8PA dielectric results in higher transistor on-current, even though the dielectric capacitance is lower than that of AlO_x.

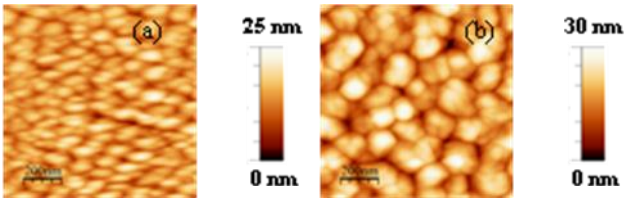

Figure 6: AFM images of pentacene deposited on AlO_x (a) and AlO_x/C_8PA (b) dielectrics. C_8PA was deposited at a rate of 7 Å/s.

4. Conclusion

To date alkyl phosphonic acid monolayers were assembled from solutions only. Our developed process provides a 'dry' alternative to the existing solution deposition, while being compatible with large-area, roll-to-roll processing. The transistors allow low-voltage operation of less than 3 V. The drain current of AlO_x/C_8PA OTFTs is 10^4 times higher than the gate leakage current, showing good electrical insulation provided by AlO_x/C_8PA bi-layer. In addition, the performance of AlO_x/C_8PA OTFTs is superior to that of AlO_x OTFTs.

The higher C_8PA evaporation rate leads to higher field-effect mobility and on/off current ratio. The off-current and subthreshold slope are reduced with increasing C_8PA evaporation rate. At the highest C_8PA evaporation rate of 7 Å/s, the highest field-effect mobility of ~ 0.061 cm^2/Vs, the threshold voltage of -1.49 V, the lowest subthreshold slope of 89 mV/decade, the minimum off-current of 1.32×10^{-12} A and the maximum on/off current ratio of ~10^6 are obtained. At present it is not clear how the evaporation rate affects the structural properties of the C_8PA monolayer, but relevant measurements are underway. Finally, we would like to mention that the developed gate dielectric is not limited to transistors based on pentacene and may be implemented in other transistor technologies.

5. Acknowledgements

The authors thank the School of Engineering of the University of Glasgow for the transistor fabrication support. This research is supported by the Scottish Funding Council through Glasgow Research Partnership in Engineering. S. Gupta is a recipient of Scottish Overseas Research Award and University Postgraduate Scholarship.

6. References

[1] V. Vaidya, S. Soggs, J. Kim, A. Haldi, J. N. Haddock, B. Kippelen, D. M. Wilson, S. Member, "Comparison of Pentacene and Amorphous Silicon AMOLED Display Driver Circuits," IEEE Trans. on Circuits and Systems I: Regular Papers, Vol. **55**, pp. 1177–1184, 2008.

[2] C. D. Sheraw, L. Zhou, J. R. Huang, D. J. Gundlach, T. N. Jackson, M. G. Kane, I. G. Hill, M. S. Hammond, J. Campi, B. K. Greening, J. Francl, J. West, "Organic Thin-Film Transistor-Driven Polymer-Dispersed Liquid Crystal Displays on Flexible Polymeric Substrates," Appl. Phys. Lett., vol. **80**, p. 1088, 2002.

[3] J. Lee, J. H. Kim, S. Im, "Effects of Substrate Temperature on the Device Properties of Pentacene-based Thin Film Transistors using Al_2O_{3+x} Gate Dielectric," J. Appl. Phys., vol. **95**, pp. 3733–3736, 2004.

[4] J. Lee, J. H. Kim, S. Im, "Pentacene Thin-Film Transistors with Al_2O_{3+x} Gate Dielectric Films Deposited on Indium-tin-Oxide Glass," Appl. Phys. Lett., vol. **83**, p. 2689, 2003.

[5] K. D. Kim, C. K. Song, "Low Voltage Pentacene Thin Film Transistors employing a Self-Grown Metal-Oxide as a Gate Dielectric," Appl. Phys. Lett., vol. **88**, p. 233508, 2006.

[6] A. Jedaa, M. Burkhardt, U. Zschieschang, H. Klauk, D. Habich, G. Schmid, M. Halik, "The Impact of Self-Assembled Monolayer Thickness in Hybrid Gate Dielectrics for Organic Thin-Film Transistors," Org. Electron., vol. **10**, pp. 1442–1447, 2009.

[7] K. Fukuda, T. Hamamoto, T. Yokota, T. Sekitani, U. Zschieschang, H. Klauk, T. Someya, "Effects of the Alkyl Chain Length in Phosphonic Acid Self-assembled Monolayer Gate Dielectrics on the Performance and Stability of Low-voltage Organic Thin-film Transistors," Appl. Phys. Lett., vol. **95**, p. 203301, 2009.

[8] U. Zschieschang, F. Ante, T. Yamamoto, K. Takimiya, H. Kuwabara, M. Ikeda, T. Sekitani, T. Someya, K. Kern, H. Klauk, "Flexible Low-Voltage Organic Transistors and Circuits based on a High-Mobility Organic Semiconductor with Good Air Stability," Adv. Mater., vol. **22**, pp. 982–985, 2010.

[9] M. Novak, C. M. Jäger, A. Rumpel, H. Kropp, W. Peukert, T. Clark, M. Halik, "The Morphology of Integrated Self-assembled Monolayers and their Impact on Devices – A Computational and Experimental Approach, Org. Electron., vol. **11**, pp. 1476–1482, 2010.

[10] P. H. Wobkenberg, J. Ball, F. B. Kooistra, J. C. Hummelen, D. M. de Leeuw, D. D. C. Bradley, T. D. Anthopoulos, "Low-voltage Organic Transistors based on Solution Processed Semiconductors and Self-assembled Monolayer Gate Dielectrics," Appl. Phys. Lett., vol. **93**, p. 013303, 2008.

[11] H. Ma, O. Acton, G. Ting, J. W. Ka, H.-L. Yip, N. Tucker, R. Schofield, A. K.-Y. Jen, "Low-Voltage Organic Thin-Film Transistors with π-σ-phosphonic Acid Molecular Dielectric Monolayers," Appl. Phys. Lett., vol. **92**, p. 113303, 2008.

[12] D. Ashall, S. J. Fakher, M. F. Mabrook, "Enhanced Performance of AlO_x-based Organic Thin-film Transistors," IEEE International Conference on Nanotechnology, pp. 61–66, 2011.

[13] K. C. Chinnam, S. Gupta, H. Gleskova, "Aluminium Oxide prepared by UV/ozone Exposure for Low-Voltage Organic Thin-Film Transistors," J. Non-Crystalline Solids, vol. **358**, pp. 2512–2515, 2012.

[14] S. Gupta, H. Gleskova, "Dry Growth of n-octylphosphonic Acid Monolayer for Low-Voltage Organic Thin-Film Transistors," Org. Electron., vol. **14**, pp. 354–361, 2013.

[15] S. Gupta, P. Šutta, D. A. Lamprou, H. Gleskova, "Effect of Substrate Temperature on Vapour-Phase Self-Assembly of n-octylphosphonic Acid Monolayer for Low-Voltage Organic Thin-Film Transistors," (to be published).

[16] H. Klauk, U. Zschieschang, J. Pflaum, M. Halik, "Ultralow-power Organic Complementary Circuits.," Nature, vol. **445**, pp. 745–748, 2007.

[17] X.-H. Zhang, W. J. Potscavage, S. Choi, B. Kippelen, "Low-voltage Flexible Organic Complementary Inverters with High Noise Margin and High dc Gain," Appl. Phys. Lett., vol. **94**, p. 043312, 2009.

[18] O. Acton, M. Dubey, T. Weidner, K. M. O'Malley, T.-W. Kim, G. G. Ting, D. Hutchins, J. E. Baio, T. C. Lovejoy, A. H. Gage, D. G. Castner, H. Ma, A. K.-Y. Jen, "Simultaneous Modification of Bottom-Contact Electrode and Dielectric Surfaces for Organic Thin-Film Transistors Through Single-Component Spin-Cast Monolayers," Adv. Func. Mater., vol. **21**, pp. 1476–1488, 2011.

[19] O. Acton, G. G. Ting, P. J. Shamberger, F. S. Ohuchi, H. Ma, A. K.-Y. K.-Y. Jen, "Dielectric Surface-Controlled Low-Voltage Organic Transistors via n-alkyl Phosphonic Acid Self-assembled Monolayers on high-k Metal Oxide.," Appl. Mater. & Interfaces, vol. **2**, pp. 511–520, 2010.